Applied Catalysis B: Environmental 230 (2018) 260–268

Contents lists available at ScienceDirect

Applied Catalysis B: Environmental

journal homepage: www.elsevier.com/locate/apcatb

One-step synthesis of nanostructured g-C_3N_4/TiO_2 composite for highly enhanced visible-light photocatalytic H_2 evolution

Yigen Tan[a], Zhu Shu[a,*], Jun Zhou[a,*], Tiantian Li[b], Wenbin Wang[a], Zhengliang Zhao[a]

[a] Faculty of Materials Science and Chemistry, Engineering Research Center of Nano-Geomaterials of Ministry of Education, China University of Geosciences, 430074 Wuhan, PR China

[b] College of Chemistry and Chemical Engineering, Henan Province Key Laboratory of Utilization of Non-metallic Mineral in the South of Henan, Xinyang Normal University, 464000 Xinyang, PR China

ARTICLE INFO

Keywords:
g-C_3N_4
TiO_2
nanocomposite
photocatalysis
hydrogen evolution

ABSTRACT

Improving the photocatalytic property of g-C_3N_4 by combined strategies has attracted increasing attention recently. In this work, we realized the structure nanosizing of g-C_3N_4 and its synchronous compounding with TiO_2 nanoparticles in one step, using a facile melamine-involved vapor deposition method coupled with a simple and easy setup. Nanostructured g-C_3N_4/TiO_2 heterojunction was well-established and the resultant nanocomposite demonstrated an excellent visible-light photocatalytic H_2 evolution performance 10.8 times higher than that of bulk g-C_3N_4. The structure nanosizing coupled with the heterojunction construction contributed together to the improvement of photoinduced electron-hole separation and final photocatalytic efficiency. The proposed simple method and setup have the potential to be used for preparing other g-C_3N_4-based nanocomposites with advanced photocatalytic properties.

1. Introduction

Environmental pollution and energy crisis are two major problems to be solved at present [1–3]. Hydrogen energy, a kind of clean energy, has attracted close attention from governments and scientists all over the world [4–6]. Photocatalytic water splitting is considered as an ideal technique for hydrogen production [7]. Among all the catalysts, nanostructured TiO_2 has been extensively studied and commercialized already, e.g. P25 [8]. However, TiO_2 only absorbs little solar photons (~5%) and hardly responds to visible light due to its large band gap of 3.2 eV [9,10]. In recent years, graphitic carbon nitride (g-C_3N_4) has been a topic of wide concern owing to its unique electronic structure and properties [11,12]. Its narrow band gap of 2.7 eV and strong visible-light absorbing ability of 460 nm make it perform well in photocatalysis [13,14]. Nevertheless, the high photogenerated electron-hole recombination rate still limits the photocatalytic efficiency.

Nano-structuring [15–17], element-doping [18,19], composite-constructing [20–22], etc. are useful strategies to improve the activity of catalysts in photocatalytic H_2 evolution. Nano-structuring primarily increases specific surface area of photocatalysts, and element-doping and composite-constructing mainly alters the electronic structure. In general, different strategy contributes in different way to improve a certain aspect of catalyst's properties [23]. Thus, the combination of multifold strategies could bring additive effect on the improvement of photocatalytic activity and becomes a new tendency in the design of advanced photocatalysts [24,25].

Over the years, constructing the composite of g-C_3N_4 and nano-TiO_2 has been proved useful to obtain enhanced performance in photocatalysis, benefiting from their appropriate band levels [26,27]. For example, Zhong et al. successfully designed a g-C_3N_4/TiO_2 heterostructure by calcining the mixture of melamine and TiO_2 nanobelt, where 2 times higher performance of H_2 evolution are obtained [28]. Wang et al. synthesized g-C_3N_4/TiO_2 by calcining their precursors, where 6 times higher performance of H_2 evolution are obtained [29]. However, the g-C_3N_4 phase of these composites is still bulk g-C_3N_4 in the micron size range. It is supposed that, if nanosized g-C_3N_4 is compounded with nano-TiO_2, the resultant nanostructured g-C_3N_4/TiO_2 composite will have a further increased efficiency in photocatalytic H_2 evolution. Several researchers have investigated the synthesis of nanostructured g-C_3N_4/TiO_2. For instance, Chen et al. controlled the growth of g-C_3N_4 on mesoporous TiO_2 spheres, resulting in a better fused g-C_3N_4/TiO_2 heterostructure [30]. Su et al. loaded g-C_3N_4 nanodots on TiO_2 nanotube arrays for better efficiency of pollutant degradation under solar light [31]. Nevertheless, the reported processes for synthesizing nanostructured g-C_3N_4/TiO_2 are generally complex, requiring two or more steps to realize the nano-structuring of g-C_3N_4

* Corresponding authors at: 388 Lumo Road, 430074 Wuhan, PR China.
E-mail addresses: shuzhu@cug.edu.cn (Z. Shu), zhoujun@cug.edu.cn (J. Zhou).

https://doi.org/10.1016/j.apcatb.2018.02.056
Received 24 December 2017; Received in revised form 6 February 2018; Accepted 25 February 2018
Available online 26 February 2018
0926-3373/

and its recombination with nano-TiO_2. Moreover, the photocatalytic H_2 evolution of the nanostructured g-C_3N_4/TiO_2 was not investigated yet and the potential influence has not been revealed. Therefore, it is still of great interest and urgency to realize the facile synthesis of nanostructured g-C_3N_4/TiO_2 composites for enhanced photocatalytic H_2 evolution.

Herein, we proposed and demonstrated a facile one-step method to achieve the nano-structuring of g-C_3N_4 and its compounding with commercialized TiO_2 nanoparticles (P25). The method was actualized via vapor deposition using an easy and simple setup. The as-obtained nanostructured g-C_3N_4/TiO_2 realized 10.8 times higher efficiency than bulk g-C_3N_4 in visible-light H_2 evolution. The detailed process was introduced, the comprehensive characterization of catalysts was conducted and the mechanism of photocatalytic activity improvement was revealed.

2. Experimental

2.1. Materials synthesis

2.1.1. Nanostructured g-C3N4/TiO2 composite

The one-step vapor deposition of nanostructured g-C_3N_4 onto TiO_2 nanoparticles was carried out using an easy and simple setup as illustrated in Scheme 1. It comprises of a covered crucible (300 mL) with a cylinder (4 cm in height) inside. In a typical experiment, 0.5 g TiO_2 nanoparticles (commercialized P25) were placed on the top of the cylinder and 24 g melamine was loaded on the bottom of the crucible. The covered crucible was put in a muffle furnace, heated at 520 °C for 4 h using a heating rate of 15 °C min^{-1} and cooled down naturally. After the above one-step treatment, the white TiO_2 powder on the cylinder top became a light-yellow powder, namely the nanostructured g-C_3N_4/TiO_2 composite. It is supposed that, yellow g-C_3N_4 grew on the surface of TiO_2 nanoparticles although they were not in touch with melamine, resulting from the sublimation feature of melamine and the gaseous phase reaction essence of polymerization reaction from melamine to g-C_3N_4 [32,33]. Different amount of melamine (4.0, 8.0, 16.0, 24.0, 30.0 and 48.0 g) were used in the experiments to adjust the amount of g-C_3N_4 depositing on TiO_2, and an increased melamine dosage leaded to an increased g-C_3N_4 deposition. The resultant products were denoted as CN/TiO_2-x, where x (= 4, 8, 16, 24, 30 or 48) represents the melamine dosage.

2.2. Control samples

For comparison, bulk g-C_3N_4 (denoted as bulk-CN) was collected from the bottom of the crucible. The nanosized g-C_3N_4 phase (denoted as nano-CN) of the g-C_3N_4/TiO_2 composite was obtained by dissolving the TiO_2 phase of CN/TiO_2-24 in hydrofluoric acid aqueous solution (40 wt%) at room temperature. A physical mixture sample of nanosized g-C_3N_4 and TiO_2 was prepared by mixing 0.051 g nano-CN with 0.049 g P25 (denoted as CN/TiO_2-mixture), which owns a weight ratio of nanosized g-C_3N_4 to TiO_2 equal to that of CN/TiO_2-24. Bulk g-C_3N_4/TiO_2 composite (denoted as bulk-CN/TiO_2) was prepared by calcining the mixture of 2 g melamine and 1 g P25, resulting in a weight ratio of g-C_3N_4 to TiO_2 similar to that of CN/TiO_2-24. A physical mixture sample of bulk g-C_3N_4 and TiO_2 was prepared by mixing 0.051 g bulk-CN with 0.049 g P25 (denoted as bulk-CN/TiO_2-mixture).

2.3. Characterization

X-ray diffraction (XRD) patterns of the samples were obtained over the diffraction angle (2θ) of 3–80° by an X-ray diffractometer with Cu Kα radiation. Fourier transform infrared (FT-IR) spectra were acquired on a Nicolet 6700 spectrometer with KBr pellet. Transmission electron microscopy (TEM) and high resolution transmission electron microscopy (HRTEM) images and the selected area electron diffraction (SAED) pattern were observed on a Tecnai G2 F20 S-TWIN electron microscope with an accelerating voltage of 200 kV. Nitrogen adsorption/desorption isotherms at 77 K were measured on a Micromeritics TriStar 3020 porosimeter. Specific surface areas of samples were calculated by the Brunauer-Emmett-Teller (BET) method. Photoluminescence (PL) spectra were obtained on an F-4500 FL spectrometer (excitation wavelength = 380 nm). UV-visible diffuse reflectance spectra (UV-vis DRS) were recorded by a Shimadzu UV-2500PC UV–vis spectrometer with the wavelength range of 240–850 nm. The photocurrent analysis was measured using photocatalyst-coated fluorine-doped tin oxide (FTO) glass with repeated on-off cycles of Xenon lamp illumination (λ > 420 nm), which was carried out using a computer-controlled potentiostat and a reference electrode of Ag/AgCl.

2.4. Photocatalytic H_2 evolution

The photocatalytic water splitting reaction was tested in a quartz reactor with top visible light irradiation. Typically, 0.1 g catalyst was dispersed in 100 mL aqueous solution containing 10 vol% sacrifice agent of triethanolamine. Then, under magnetic stirring, 10 mL triethanolamine was added as sacrificial electron donor and 1 mL H_2PtCl_6 aqueous solution was added to preset the mass ratio of Pt cocatalyst to photocatalyst at 3 wt%. The vessel was purged by N_2 for 0.5 h to remove air, sealed with a rubber stopper and then irradiated for 1 h under visible light using a 300 W Xe lamp with a cut-off filter (λ > 420 nm) at the fixed light-to-liquid distance (10 cm) to photo-reduce H_2PtCl_6 into Pt cocatalyst. Finally, the sealed reactor was irradiated under the same visible light after thoroughly purging the system with nitrogen again, and the reaction temperature was maintained at 283 K by cyclical cooling water. 1 mL gas was sampled every one hour and the hydrogen content was analyzed by a gas chromatograph with a thermal conductivity detector. After reacting for 4 h, the quartz reaction vessel was purged by nitrogen again. The reaction process was repeated for four runs.

2.5. Apparent quantum efficiency (AQE) measurement

The apparent quantum efficiency (AQE) was measured using the water splitting experimental setup under the irradiation of monochromatic light (λ = 420 nm) and calculated by the formula (1) [34–36]:

$$AQE = \frac{n \times \Delta G}{I} \times 100\% = \frac{n \times \Delta G}{W \times S \times t} \times 100\% \quad (1)$$

where n stands for the mole number of H_2 evolution; ΔG = 237 kJ mol^{-1}, that is the needed energy of one molecule water

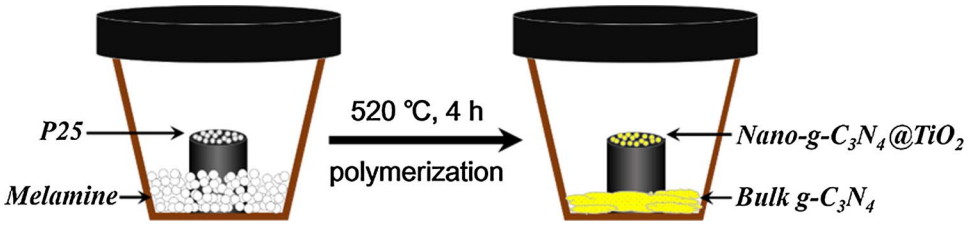

Scheme 1. Schematic illustration of the one-step synthesis of nanostructured g-C_3N_4/TiO_2 composite via facial melamine-involved vapor deposition.

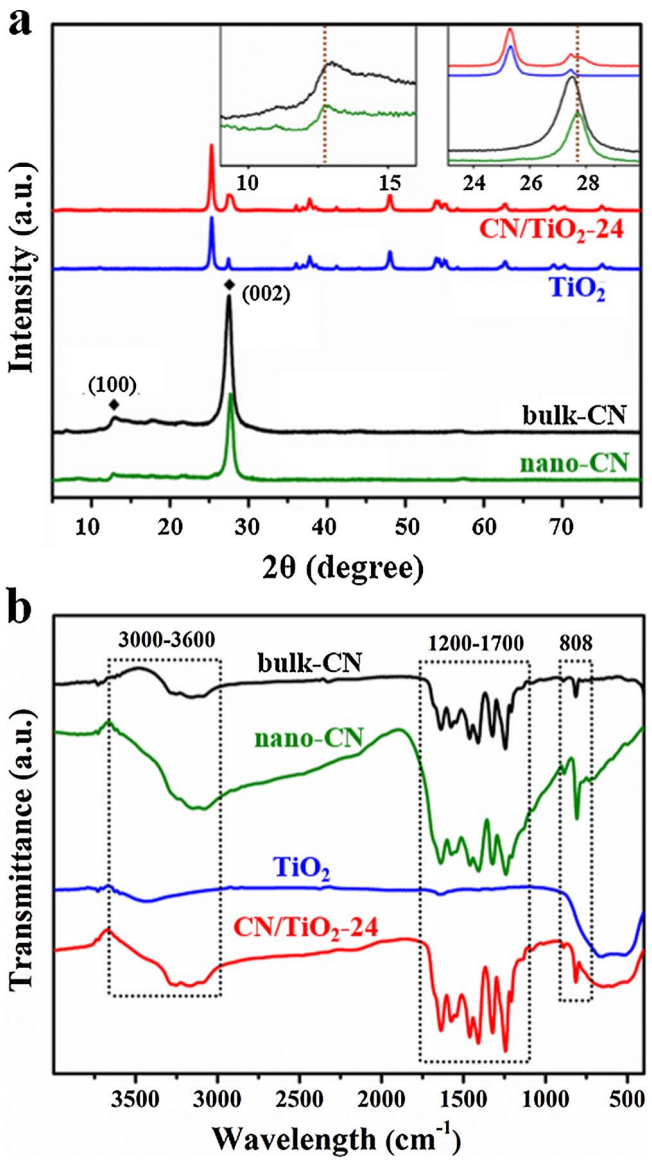

Fig. 1. (a) XRD patterns and local magnifications (inserts) and (b) FT-IR spectra of CN/TiO_2-24, TiO_2, bulk-CN and nano-CN.

entirely splitting into H_2 and O_2; W is the power of lamp; S represents the irradiated area; t is the reaction time.

3. Results and discussion

3.1. Formation of nanostructured g-C_3N_4/TiO_2 composite

The XRD pattern of as-synthesized CN/TiO_2-24 is shown in Fig. 1a in comparison with those of control samples: TiO_2 and bulk-CN. Obviously, CN/TiO_2-24 is a composite of TiO_2 and g-C_3N_4. For detailed comparison, the g-C_3N_4 phase (nano-CN) of CN/TiO_2-24 was abstracted by removing the TiO_2 phase from CN/TiO_2-24 and its XRD pattern is exhibited in Fig. 1a. It can be seen that, the peak locations belonging to the g-C_3N_4 phase of CN/TiO_2-24 (nano-CN) are slightly different from those of bulk-CN. Bulk-CN exhibits two characteristic diffraction peaks of g-C_3N_4 at $2\theta = 12.7^\circ$ and 27.5°, which correspond to the in-plane repeating of N-bridged tri-s-triazine units ((100) plane diffraction) and the inter-planar stacking of conjugated aromatic system ((002) plane diffraction), respectively. Compared with bulk-CN, nano-CN owns a similar XRD pattern with relatively lower peaks, suggesting that nano-CN is composed of g-C_3N_4 with reduced sizes. Moreover, the (002) reflection peak of g-C_3N_4 right-shifts from 27.5° for bulk-CN to 27.8° for nano-CN and CN/TiO_2-24, implying a 0.003 nm decrease of interlayer distance between the unit layers of g-C_3N_4 in CN/TiO_2-24. The (100) peak down-shifts from 12.9° for bulk-CN to 12.7° for nano-CN and CN/TiO_2-24, corresponding to a 0.014 nm increase of the in-plane hole-to-hole distance, which means that the unit layer of g-C_3N_4 in CN/TiO_2-24 has become more planarized. The planarization of g-C_3N_4 unit layers is beneficial for the delocalization of π electrons, thus the interaction of π-π stacking is enhanced and leads to the decreasing of interlayer spacing [37]. These crystal structure differences between the g-C_3N_4 phase of CN/TiO_2-24 and the bulk g-C_3N_4 preliminarily indicate the nanosizing of g-C_3N_4 in CN/TiO_2-24, which will get further proofs in subsequent analysis.

The FT-IR spectra of bulk-CN, nano-CN, TiO_2 and CN/TiO_2-24 are shown in Fig. 1b. Data shows that the spectra of CN/TiO_2-24 is a combination of those of TiO_2 and g-C_3N_4. Specifically, the absorption band between 600 and 800 cm^{-1} denotes the stretching vibration of Ti-O-Ti. The sharp absorption peak at 808 cm^{-1} is attributed to the out-of-plane bending vibration of tri-s-triazine units of g-C_3N_4. The intense absorption band between 1200 and 1700 cm^{-1} is ascribed to the typical C-N and C=N stretching vibration of tri-s-triazine rings, and the wide absorption band between 3000 and 3600 cm^{-1} is due to the stretching vibration of terminal −NH groups of g-C_3N_4. It is remarkable that, the characteristic vibration peaks related to the g-C_3N_4 phase in both CN/TiO_2-24 and its nano-CN counterpart are much sharper than those of bulk-CN, which can be attributed to their crystal structural difference. As discussed above, the unit layers of the g-C_3N_4 phase in CN/TiO_2-24 are more planarized in comparison with bulk-CN, which leads to the separation of atoms in two neighbor tri-s-triazine rings and thus weakens their interaction. Hence, the atoms in the g-C_3N_4 phase of CN/TiO_2-24 vibrate more strongly due to the reduced constraint.

Fig. 2 exhibits the TEM-observed microstructure of CN/TiO_2-24 and reference samples. As shown in Fig. 2a, P25 is composed of typical TiO_2 nanoparticles of 10 ~ 20 nm in diameter. After the melamine-involved vapor deposition treatment, all the TiO_2 nanoparticles are wrapped by nanoscale g-C_3N_4 with a thickness of about 20 nm as shown by the TEM observations with different magnifications in Fig. 2b, c, forming a nanostructured g-C_3N_4/TiO_2 composite (CN/TiO_2-24). The HRTEM image of CN/TiO_2-24 nanocomposite in Fig. 2d shows the clear lattice fringes of TiO_2 (d = 0.35 nm corresponding to TiO_2 (101)) coupled with the intimate vague fringes of g-C_3N_4 [38–40]. The observed intimate contact between g-C_3N_4 and TiO_2 enables the formation of surface hybrid heterojunction which is conductive to charge separation [41]. The selected area electron diffraction (SAED) pattern of CN/TiO_2-24 also shows that the composite is polycrystalline in nature. These results point out that the nanostructured g-C_3N_4/TiO_2 heterojunction is well established. When the TiO_2 phase of CN/TiO_2-24 is removed, the resultant pure g-C_3N_4 phase (nano-CN) clearly shows a nanoporous morphology (Fig. 2e). By contrast, the traditional bulk-CN sample consists of thick granules of micron size (Fig. 2f). N_2 adsorption-desorption analysis (Fig. 2 g, h) further demonstrates that CN/TiO_2-24 owns a nanosized structure and nano-CN owns a mesoporous structure with favorable specific surface areas (67.1 $m^2 g^{-1}$ for CN/TiO_2-24 and 77.5 $m^2 g^{-1}$ for nano-CN) about 11 and 13 times higher than that of bulk-CN (6.1 $m^2 g^{-1}$), respectively. Meanwhile, the specific surface area of CN/TiO_2-24 is much higher than that of the TiO_2 nanoparticles (42.2 $m^2 g^{-1}$), while the sample bulk-CN/TiO_2 synthesized by directly mixing and calcining their precursors owns a much lower specific surface area (21.5 $m^2 g^{-1}$). These results fully demonstrate the advantage of the proposed vapor deposition method in the construction of g-C_3N_4/TiO_2 nanocomposite with enlarged specific surface area. In short, the TEM/HRTEM observations and N_2 adsorption-desorption results accord well with the XRD and FT-IR results, all of which point to the successful construction of nanostructured g-C_3N_4/TiO_2 heterojunction via the facial one-pot vapor deposition process.

The surface chemical compositions of bulk-CN, TiO_2 and CN/TiO_2-

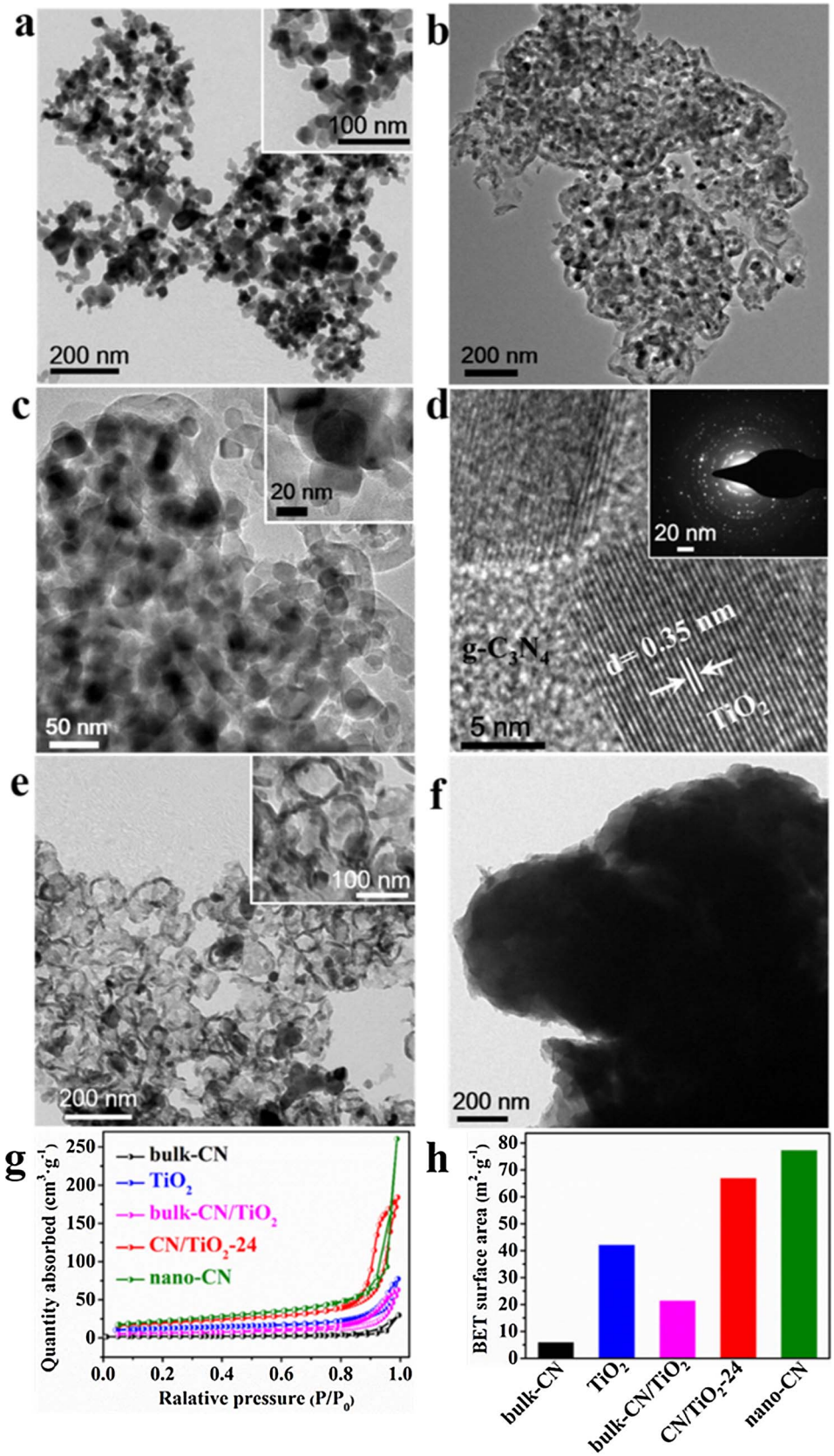

Fig. 2. (a) TEM image of TiO_2; (b, c) TEM images and (d) HRTEM image (insert is SAED pattern) of CN/TiO_2-24; TEM images of (e) nano-CN and (f) bulk-CN; (g) N_2 adsorption-desorption isotherm curves and (h) BET specific surface areas of bulk-CN, TiO_2, bulk-CN/TiO_2, CN/TiO_2-24 and nano-CN.

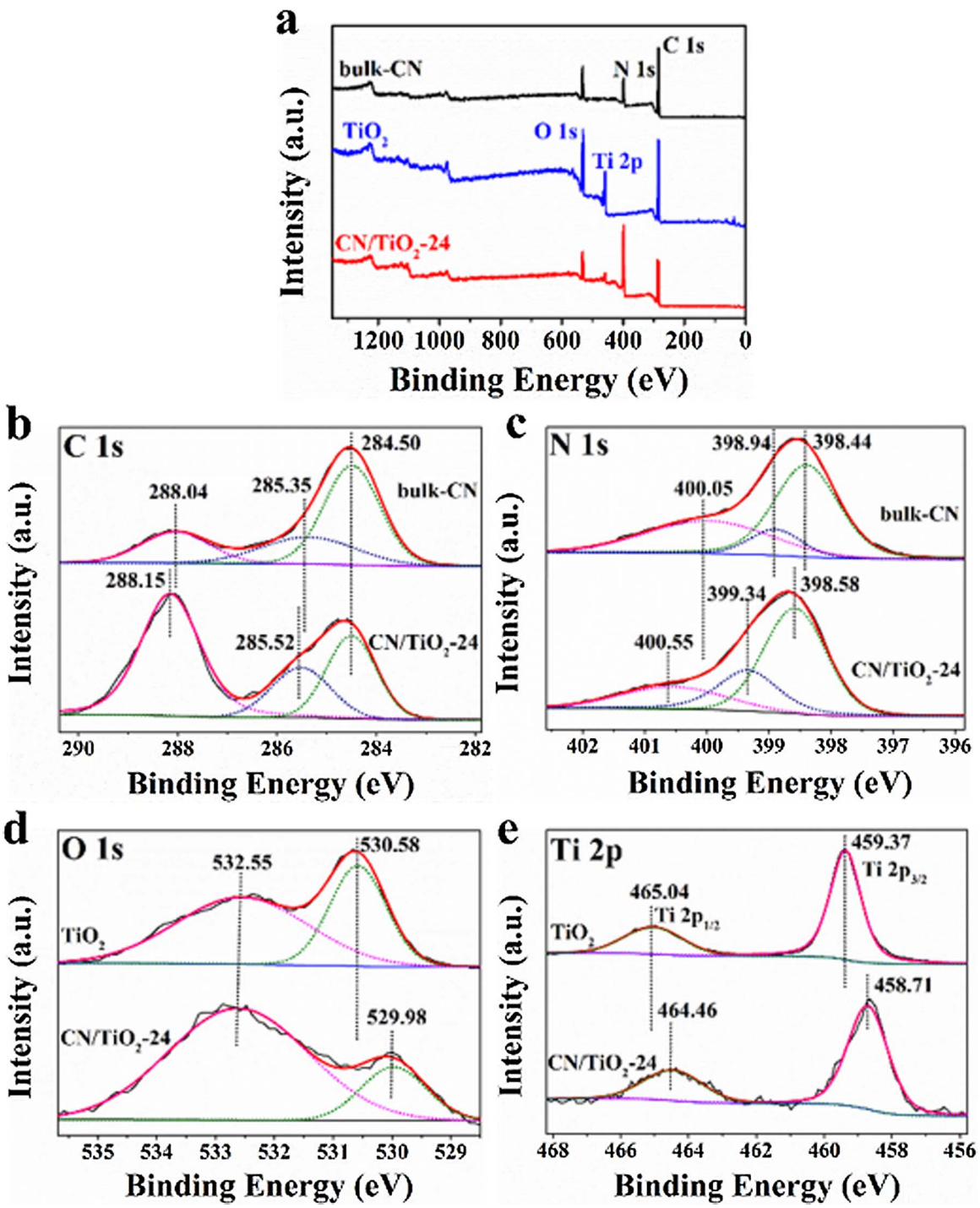

Fig. 3. Survey and high-resolution XPS spectra of bulk-CN, TiO_2 and CN/TiO_2-24. (a) Survey spectra; (b) C 1 s spectra of bulk-CN and CN/TiO_2-24; (c) N 1 s spectra of bulk-CN and CN/TiO_2-24; (d) O 1 s spectra of TiO_2 and CN/TiO_2-24; (e) Ti 2p spectra of TiO_2 and CN/TiO_2-24.

24 samples were measured by X-ray photoelectron spectroscopy. As we can see from Fig. 3a, all elements including C, N, O and Ti are detected in the survey spectra of CN/TiO_2-24, which implies that the composite is mainly composed of C, N, O and Ti elements. It should be noted that O was found in bulk-CN due to the adsorbed hydroxyl groups and C was found in pure TiO_2 due to the surface adventitious carbon from XPS instrument itself. Fig. 3b presents the corresponding high-resolution C1 s spectra of bulk-CN and CN/TiO_2-24. The C 1 s spectrum can be deconvoluted into three different Gaussian-Lorentzian peaks centered at the binding energies of 284.50, 285.35 and 288.04 eV. The peak at 284.50 eV is attributed to the C-C coordination of the surface adventitious carbon; the peak at 285.35 eV is attributed to the C═N groups; and the peak at 288.04 eV is attributed to C-N or C-$(N)_3$ groups [42]. The C 1 s spectrum of CN/TiO_2-24 was similar to that of bulk-CN, but the peak of C═N and C-N shifted 0.11 and 0.17 eV towards higher binding energy, respectively. In the N 1 s spectrum of bulk-CN (Fig. 3c), three peaks can be observed after deconvolution. The peak at 398.44 eV is attributed to sp^2-hybridized aromatic N (C═N-C); the peak at 398.94 eV is attributed to tertiary nitrogen N-$(C)_3$; the peak at 400.05 eV is attributed to C-N-H groups [43]. These peaks have a shift of 0.14, 0.40 and 0.50 eV towards higher binding energy, respectively. In the O 1 s spectrum of TiO_2 (Fig. 4d), the peak at 530.58 eV is

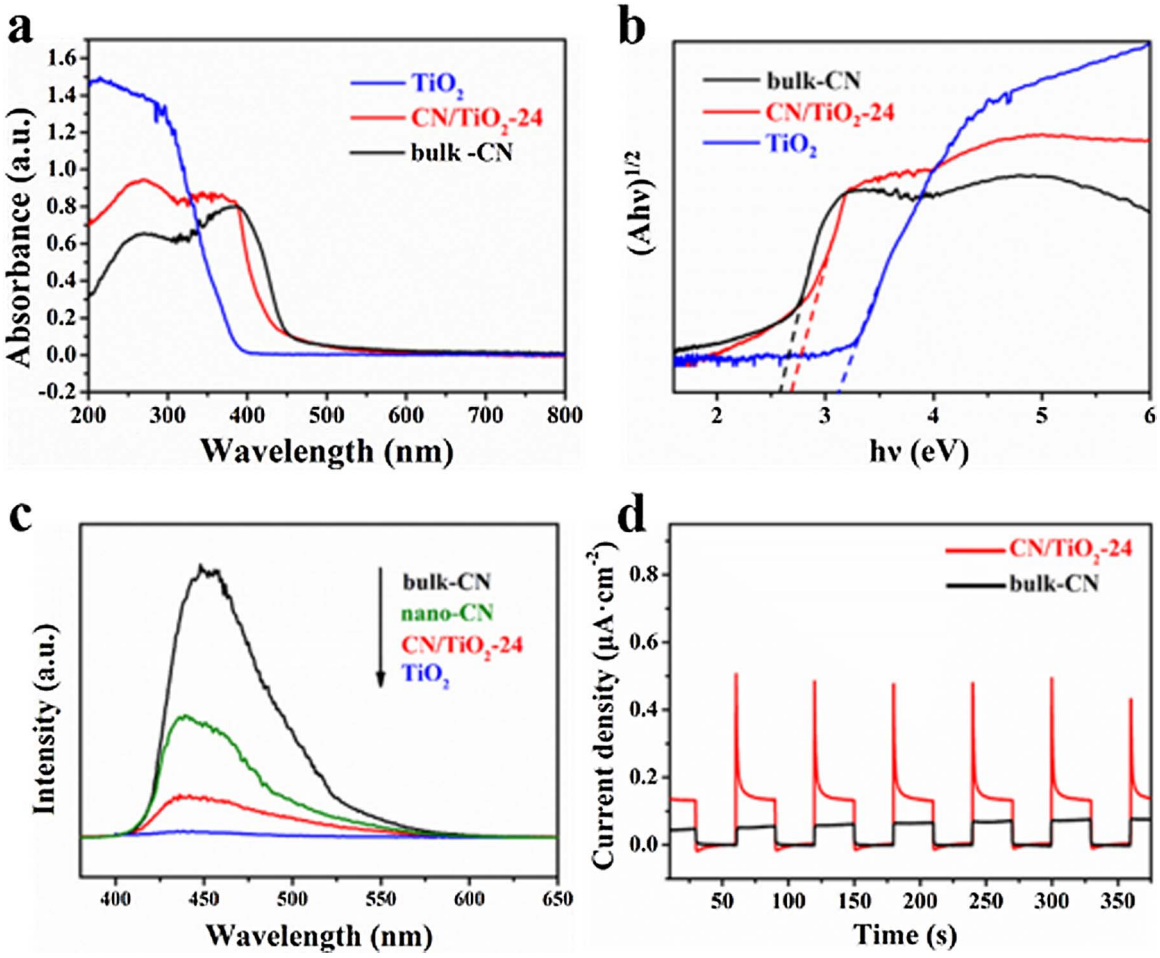

Fig. 4. (a) UV–vis DRS spectra and (b) Kubelka-Munk transformed function of TiO_2, CN/TiO_2-24 and bulk-CN; (c) PL spectra of bulk-CN, nano-CN, CN/TiO_2-24 and TiO_2; (d) Transient photocurrent responses of CN/TiO_2-24 and bulk-CN.

attributed to the Ti-O band; the peak at 532.55 eV is attributed to the surface −OH groups [44]. Nevertheless, the peak of Ti-O shifts 0.60 eV towards lower binding energy in O 1 s spectrum of CN/TiO_2-24. In the Ti 2p spectrum (Fig. 3e), the two peaks at 459.37 and 465.04 eV of TiO_2 correspond to the Ti $2p_{3/2}$ and Ti $2p_{1/2}$, respectively, while the peaks of CN/TiO_2-24 shifts 0.66 and 0.58 eV towards lower binding energy, respectively [45]. The up-shifts of C 1 s and N 1 s peaks and the down-shifts of O 1 s and Ti 2p peaks of CN/TiO_2-24 can be attributed to the chemical environment change arising from the close interaction between g-C_3N_4 and TiO_2 [46–48], which again demonstrates the well establishment of g-C_3N_4/TiO_2 heterojunction in CN/TiO_2-24.

3.2. Optical characteristics

UV-Vis diffuse reflectance spectrometer was used to study the optical absorption properties of these samples. Fig. 4a indicates that bulk-CN has an absorption edge at 465 nm, while CN/TiO_2-24 shows a blue shift toward shorter wavelength (~ 425 nm). The blue shift of absorption edge results from the increase of band gap of semiconductors. As plotted in Fig. 4b, the estimated band gap value is 2.65 and 2.75 for bulk-CN and CN/TiO_2-24, respectively, according to the converted curve of Kubelka-Munk function versus light energy. The increased band gap of CN/TiO_2-24 compared with bulk-CN can be attributed to the well-known quantum size effect in nanomaterials, namely, the band gap of g-C_3N_4 phase increases with the decrease of its crystal size into nanoscale. Besides, the light absorption of CN/TiO_2-24 is still much boarder than that of TiO_2 with a typical large band gap of 3.17 eV. The existence of g-C_3N_4 phase in the composite is believed to contribute to its superior optical absorption.

The photoluminescence (PL) spectroscopy reveals the recombination degree of photogenerated electron-hole pairs and a high emission intensity means a great recombination probability. Fig. 4b exhibits the PL emission spectra of bulk-CN, nano-CN, TiO_2 and CN/TiO_2-24 at 380 nm excitation. Bulk-CN shows a strong peak at 455 nm, corresponding to the energy of radiant light approximately equal to the narrow band gap energy of g-C_3N_4 (2.65 eV). Compared with bulk-CN, the emission intensity of nano-CN is significantly weaker, demonstrating its lower rate of electron-hole recombination. Besides, the PL emission peak down-shifts slightly from 455 nm for bulk-CN to 438 nm for nano-CN, which corresponds to the enlarging of band gap from 2.65 eV for bulk-CN to 2.75 eV for nano-CN. It is interesting that, when nano-CN combines with P25 to form the nanostructured g-C_3N_4/TiO_2 composite (CN/TiO_2-24), the emission intensity further decreases substantially, indicating that the charge carrier recombination is effectively impeded because of the efficient charge separation and transfer from g-C_3N_4 to TiO_2 via heterojunction interface. Additionally, there is hardly PL emission for TiO_2 in the range of 380 ~ 650 nm, since no electron can be excited by 380 nm photon due to its large band gap (3.17 eV).

On the other hand, photocurrent density analysis, a well-known important evidence for demonstrating charge separation and migration, was employed to further investigate the separation efficiency of photoinduced carriers in the nanocomposite. As plotted in Fig. 4d, CN/TiO_2-24 shows a photocurrent density response obviously higher than that of bulk-CN, which again manifests that the separation and transfer efficiency of photoinduced electro-hole pairs is increased in the nanostructured g-C_3N_4/TiO_2 composite.

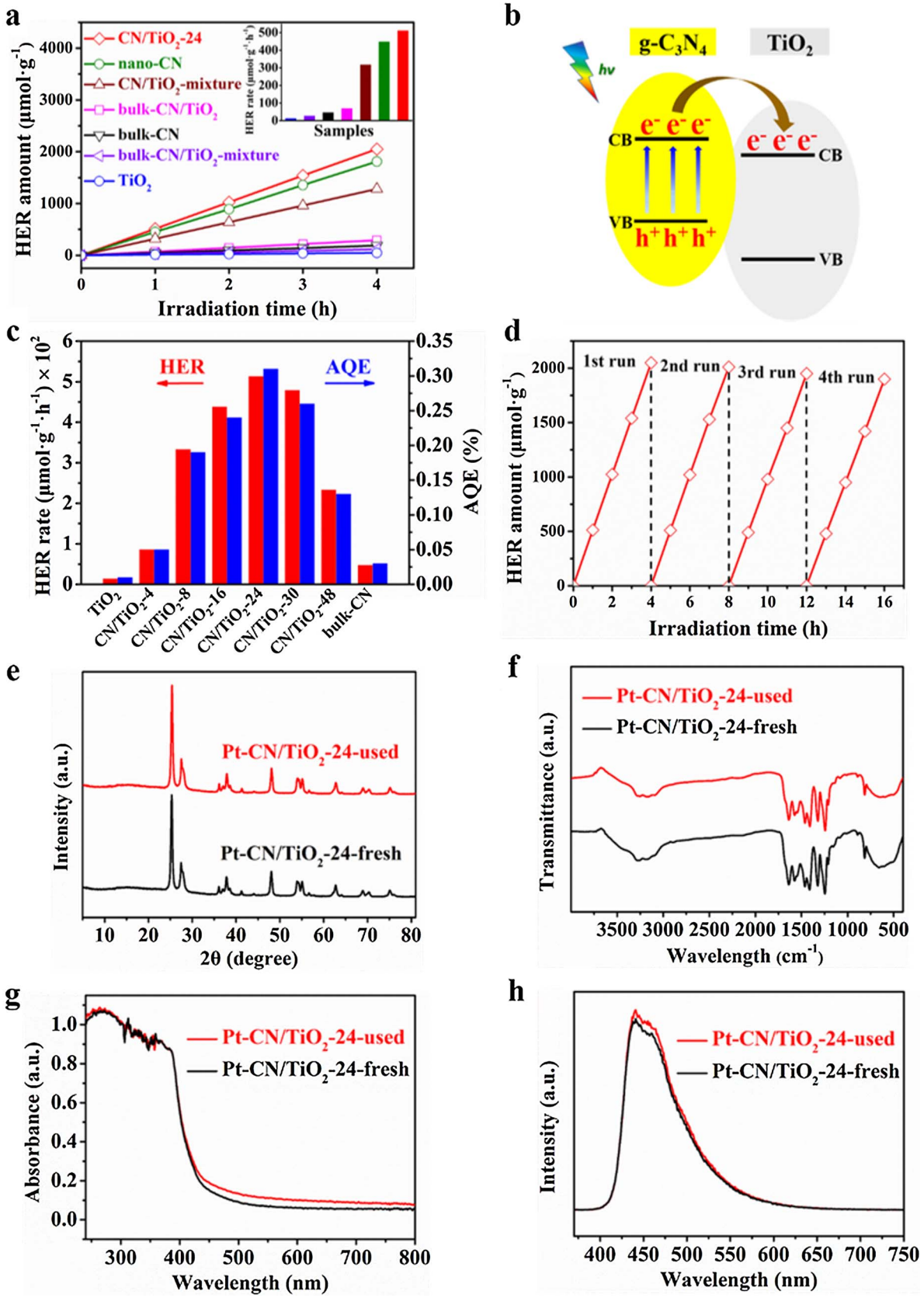

Fig. 5. (a) Time courses of H_2 evolution on CN/TiO_2-24, nano-CN, CN/TiO_2-mixture, bulk-CN/TiO_2, bulk-CN, bulk-CN/TiO_2-mixture and TiO_2; insert is the H_2 evolution rates; (b) Schematic diagram of electronic transfer mechanism; (c) H_2 evolution rates and AQE values of TiO_2, CN/TiO_2-4, −8, −16, −24, −30 and −48, and bulk-CN; (d) Recycling tests of CN/TiO_2-24; (e) XRD patterns, (f) FT-IR, (g) UV–vis DRS and (h) PL spectra of the catalyst before and after H_2 evolution test.

3.3. Visible-light photocatalytic performance

The visible-light photocatalytic activity of the samples was evaluated by H_2 evolution reaction (HER) under visible light. Fig. 5a displays the time course and average rate of visible-light H_2 evolution on CN/TiO_2-24 in composition with the control samples. Data shows that, all samples except TiO_2 is capable of obvious H_2 evolution under visible light, because TiO_2 nanoparticles are negative in visible-light absorption (Fig. 4a). Bulk-CN generates H_2 at the rate of 47.4 μmol g^{-1} h^{-1}. When bulk-CN is physically mixed with the TiO_2 nanoparticles, the obtained sample bulk-CN/TiO_2-mixture produces H_2 at an even reduced rate of 28.5 μmol g^{-1} h^{-1}, due to both the visible-light inertness of TiO_2 and the absence of g-C_3N_4/TiO_2 heterojunction in the physical mixture. When combining bulk-CN with TiO_2 to form a composite by pre-mixing and calcining their precursors, the resultant bulk-CN/TiO_2 shows a H_2 evolution rate of 71.5 μmol g^{-1} h^{-1} slightly higher than that of bulk-CN, benefitting from the constructed g-C_3N_4/TiO_2 heterojunction. On the other hand, the physical mixture of nano-CN and TiO_2 (CN/TiO_2-mixture) and nano-CN show substantially enhanced H_2 evolution rate of 319 μmol g^{-1} h^{-1} and 450 μmol g^{-1} h^{-1}, respectively, representing the contribution of the nanosizing of g-C_3N_4 on its visible-light photocatalytic activity. What is more, when the nanoscale g-C_3N_4 and TiO_2 combine to form the nanostructured g-C_3N_4/TiO_2 composite (CN/TiO_2-24), a further improved H_2 evolution rate of 513 μmol g^{-1} h^{-1} is realized, which is 10.8 times higher than bulk-CN and much superior to CN/TiO_2-mixture. These results suggest that, both the nanosizing of g-C_3N_4 phase and the well-established heterojunction of nanoscale g-C_3N_4 and TiO_2 in CN/TiO_2-24 have contributed to its improvement in visible-light photocatalytic H_2 evolution.

Specifically, compared with bulk g-C_3N_4, the nanosized g-C_3N_4 with increased specific surface area can absorb greater amount of light in unit time thus generate more photoinduced charge carriers. Moreover, the greatly enlarged specific surface area of nanosized g-C_3N_4 can provide much more active sites for photo-induced electrons and holes to participate in catalytic reaction, and the recombination of electron and hole can be suppressed efficiently. Furthermore, as well-known and illustrated in Fig. 5b, when g-C_3N_4 combines with TiO_2 to construct an II-type heterojunction, the visible-light-excited electrons in the conduction band (CB) of g-C_3N_4 can transfer into the CB of TiO_2, realizing a further enhanced separation of photoinduced charge carriers [49–51]. In short, the nanosizing of g-C_3N_4 and its association with TiO_2 synergistically suppress the recombination of photoinduced charge carriers and improve the visible-light photocatalytic H_2 evolution of CN/TiO_2-24.

Fig. 5c shows the calculated average visible-light H_2 evolution rate and apparent quantum efficiency (AQE, under 420 nm) of several nanostructured g-C_3N_4/TiO_2 composites (CN/TiO_2-x) with different content of g-C_3N_4, which was determined by thermogravimetric (TG) measurement (shown in Fig. S1 in Supporting Information). It can be seen that, the visible-light H_2 evolution efficiency of the composite increases upon enlarging the g-C_3N_4 content from 12.5 wt% to 51.5 wt % and then decreases at further enlarged g-C_3N_4 content. The AQE of CN/TiO_2-x also varies with the g-C_3N_4 content, which follows the same trend as that of the H_2 evolution rate. The optimal sample, CN/TiO_2-24, shows the maximum AQE value of 0.31% that is 11.3 times greater than that of bulk-CN (0.027%). The increase of activity at the beginning can be attributed to the increase of g-C_3N_4 content in the composite, because g-C_3N_4 is the only phase absorbing visible light. However, a larger g-C_3N_4 content also means the deposition of a thicker g-C_3N_4 phase, which possesses a worse efficiency for the separation of photoinduced charge carriers. At the same time, the decrease of TiO_2 content, corresponding to the increase of g-C_3N_4 content, indicates the reduction of g-C_3N_4/TiO_2 heterojunction interface that is extremely important for photoinduced electron-hole separation. Therefore, the excessive deposition of g-C_3N_4 on TiO_2 (g-C_3N_4 content above 51.5 wt%) leads to the decrease of visible-light photocatalytic activity of the g-C_3N_4/TiO_2 nanocomposite.

For further comparison, some other reported g-C_3N_4/TiO_2 composites were also prepared according to literatures [28,29]. The synthesis procedures are detailed in the Supporting Information, and the time course of visible-light H_2 evolution on the samples were plotted in Fig. S2. The average H_2 evolution rate of these reported optimal composites are calculated to be below 261 μmol g^{-1} h^{-1} (shown in Fig. S3 in the Supporting Information), which is much smaller than that of CN/TiO_2-24 (513 μmol g^{-1} h^{-1}). It can be found that the proposed vapor deposition method is easier-to-handle and the as-prepared CN/TiO_2-24 is much superior in visible-light photocatalytic H_2 evolution.

In addition, the stability of photocatalyst is also an important index to evaluate photocatalytic activity. The recycling test of H_2 evolution was carried out at the same experiment condition. As shown in Fig. 5d, the CN/TiO_2-24 sample displays steady H_2 evolution for four runs (16 h in total) without apparent deactivation, indicating a favorable photocatalytic stability. For further proof, the fresh sample loaded with Pt without H_2 evolution test (denoted as Pt-CN/TiO_2-24-fresh) and the used counterpart after H_2 evolution testing for four runs (denoted as Pt-CN/TiO_2-24-used) were collected for further characterization. Data shows that, there is few difference in the XRD pattern (Fig. 5e), FT-IR (Fig. 5f), UV–vis DRS (Fig. 5 g) and PL (Fig. 5 h) spectra of the sample before and after the H_2 evolution test, further suggesting that the catalyst is relatively stable in visible-light photocatalytic H_2 evolution.

4. Conclusion

Nanostructured g-C_3N_4/TiO_2 composites were synthesized by controlling the growth of nanoscale g-C_3N_4 on TiO_2 nanoparticles via a facile one-step melamine-involved vapor deposition method using an easy and simple setup. The nanosizing of g-C_3N_4 and its good interfacial connection with TiO_2 promote both visible light absorption and photogenerated electron transfer and separation. The g-C_3N_4 content can be adjusted and the optimal g-C_3N_4/TiO_2 nanocomposite presents a favorable visible-light photocatalytic H_2 evolution efficiency that is 10.8 times superior to bulk g-C_3N_4. The established simple method and setup provide more opportunities for the design and facial synthesis of g-C_3N_4-based nanocomposites.

Acknowledgements

The authors gratefully acknowledge the support from the National Natural Science Foundation of China (41502030, 51502272), the Zhejiang Provincial Natural Science Foundation of China (LQY18D020001), the Fundamental Research Funds for the Central Universities, the Open Foundation of Engineering Research Center of Nano-Geomaterials of Ministry of Education (NGM2017KF008) and Hubei Environmental Protection Bureau (2013HB10). The helpful comments of two anonymous reviewers are also highly acknowledged.

Appendix A. Supplementary data

Supplementary data associated with this article can be found, in the online version, at https://doi.org/10.1016/j.apcatb.2018.02.056.

References

[1] C. Han, Y. Wang, Y. Lei, B. Wang, N. Wu, Q. Shi, Q. Li, In situ synthesis of graphitic-C_3N_4 nanosheet hybridized N-doped TiO_2 nanofibers for efficient photocatalytic H_2 production and degradation, Nano Res. 8 (2015) 1199–1209.
[2] X. Wei, C. Shao, X. Li, N. Lu, K. Wang, Z. Zhang, Y. Liu, Facile in situ synthesis of plasmonic nanoparticles-decorated g-C_3N_4/TiO_2 heterojunction nanofibers and comparison study of their photosynergistic effects for efficient photocatalytic H_2 evolution, Nanoscale 8 (2016) 11034–11043.
[3] J. He, L. Chen, Z.Q. Yi, C.T. Au, S.F. Yin, CdS nanorods coupled with WS_2 nanosheets for enhanced photocatalytic hydrogen evolution activity, Ind. Eng. Chem. Res. 55 (2016) 8327–8333.
[4] B. Chai, T. Peng, J. Mao, K. Li, L. Zan, Graphitic carbon nitride (g-C_3N_4)-Pt-TiO_2

nanocomposite as an efficient photocatalyst for hydrogen production under visible light irradiation, Phys. Chem. Chem. Phys. 14 (2012) 16745–16752.
[5] G. Li, Z. Lian, W. Wang, D. Zhang, H. Li, Nanotube-confinement induced size-controllable g-C_3N_4 quantum dots modified single-crystalline TiO_2 nanotube arrays for stable synergetic photoelectrocatalysis, Nano Energy 19 (2016) 446–454.
[6] J. He, L. Chen, F. Wang, Y. Liu, P. Chen, C.T. Au, S.F. Yin, CdS nanowires decorated with ultrathin MoS_2 nanosheets as an efficient photocatalyst for hydrogen evolution, ChemSusChem. 9 (2016) 624–630.
[7] H. Hou, F. Gao, L. Wang, M. Shang, Z. Yang, J. Zheng, W. Yang, Superior thoroughly mesoporous ternary hybrid photocatalysts of TiO_2/WO_3/g-C_3N_4 nanofibers for visible-light-driven hydrogen evolution, J. Mater. Chem. A 4 (2016) 6276–6281.
[8] Y. Chen, W. Huang, D. He, S. Yue, H. Huang, Construction of heterostructured g-C_3N_4/Ag/TiO_2 microspheres with enhanced photocatalysis performance under visible-light irradiation, ACS. Appl. Mater. Inter. 6 (2014) 14405–14414.
[9] K. Li, S. Gao, Q. Wang, H. Xu, Z. Wang, B. Huang, Y. Dai, J. Lu, In-situ-reduced synthesis of Ti^{3+} self-doped TiO_2/g-C_3N_4 heterojunctions with high photocatalytic performance under LED light irradiation, ACS. Appl. Mater. Inter. 7 (2015) 9023–9030.
[10] S. Sun, M. Sun, Y. Fang, Y. Wang, H. Wang, One-step in situ calcination synthesis of g-C_3N_4/N-TiO_2 hybrids with enhanced photoactivity, RSC Adv. 6 (2016) 13063–13071.
[11] J. Zhang, M. Zhang, R.-Q. Sun, X. Wang, A facile band alignment of polymeric carbon nitride semiconductors to construct isotype heterojunctions, Angew. Chem. Int. Ed. 51 (2012) 10145–10149.
[12] Y. Zeng, X. Liu, C. Liu, L. Wang, Y. Xia, S. Zhang, S. Luo, Y. Pei, Scalable one-step production of porous oxygen-doped g-C_3N_4 nanorods with effective electron separation for excellent visible-light photocatalytic activity, Appl. Catal. B 224 (2018) 1–9.
[13] I. Papailias, N. Todorova, T. Giannakopoulou, J. Yu, D. Dimotikali, C. Trapalis, Photocatalytic activity of modified g-C_3N_4/TiO_2 nanocomposites for NOx removal, Catal. Today 280 (2017) 37–44.
[14] C. Li, Z. Sun, W. Zhang, C. Yu, S. Zheng, Highly efficient g-C_3N_4/TiO_2/kaolinite composite with novel three-dimensional structure and enhanced visible light responding ability towards ciprofloxacin and S. aureus, Appl. Catal. B 220 (2017) 272–282.
[15] J.S. Zhang, F.S. Guo, X.C. Wang, An optimized and general synthetic strategy for fabrication of polymeric carbon nitride nanoarchitectures, Adv. Mater. 23 (2013) 3008–3014.
[16] Y.S. Jun, W.H. Hong, M. Antonietti, A. Thomas, Mesoporous, 2D hexagonal carbon nitride and titanium nitride/carbon composites, Adv. Mater. 21 (2009) 4270–4274.
[17] J. He, L. Chen, Z.Q. Yi, D. Ding, C.T. Au, S.F. Yin, Fabrication of two-dimensional porous CdS nanoplates decorated with C_3N_4 nanosheets for highly efficient photocatalytic hydrogen production from water splitting, Catal. Commun. 99 (2017) 79–82.
[18] S.W. Hu, L.W. Yang, Y. Tian, X.L. Wei, J.W. Ding, J.X. Zhong, P.K. Chu, Simultaneous nanostructure and heterojunction engineering of graphitic carbon nitride via in situ Ag doping for enhanced photoelectrochemical activity, Appl. Catal. B 163 (2015) 611–622.
[19] J. Zhao, L., Ma, H., Wang, Y., Zhao, J., Zhang, S. Hu, Novel band gap-tunable K–Na co-doped graphitic carbon nitride prepared by molten salt method, Appl. Surf. Sci. 332 (2015) 625-630.
[20] K.C. Christoforidis, T. Montini, E. Bontempi, S. Zafeiratos, J.J. Delgado Jaen, P. Fornasiero, Synthesis and photocatalytic application of visible-light active beta-Fe_2O_3/g-C_3N_4 hybrid nanocomposites, Appl. Catal. B 187 (2016) 171–180.
[21] X.Y. Yuan, C. Zhou, Q.Y. Jing, Q. Tang, Y.H. Mu, A.K. Du, Facile synthesis of g-C_3N_4 nanosheets/ZnO nanocomposites with enhanced photocatalytic activity in reduction of aqueous chromium(VI) under visible light, Nanomaterials 6 (2016) 12.
[22] Q. Li, X. Li, S. Wageh, A.A. Al-Ghamdi, J.G. Yu, CdS/graphene nanocomposite photocatalysts, Adv. Energy. Mater. 5 (2015) 28.
[23] X.J. Bai, S.C. Yan, J.J. Wang, L. Wang, W.J. Jiang, S.L. Wu, C.P. Sun, Y.F. Zhu, A simple and efficient strategy for the synthesis of a chemically tailored g-C_3N_4 material, J. Mater. Chem. A 2 (2014) 17521–17529.
[24] M.J. Munoz-Batista, A. Kubacka, M. Fernandez-Garcia, Effect of g-C_3N_4 loading on TiO_2-based photocatalysts: UV and visible degradation of toluene, Catal. Sci. Technol. 4 (2014) 2006–2015.
[25] Y.X. Wang, H. Wang, F.Y. Chen, F. Cao, X.H. Zhao, S.G. Meng, Y.J. Cui, Facile synthesis of oxygen doped carbon nitride hollow microsphere for photocatalysis, Appl. Catal. B 206 (2017) 417–425.
[26] H. Tang, S. Chang, L. Jiang, G. Tang, W. Liang, Novel spindle-shaped nanoporous TiO_2 coupled graphitic g-C_3N_4 nanosheets with enhanced visible-light photocatalytic activity, Ceram. Int. 42 (2016) 18443–18452.
[27] C. Li, Z. Sun, Y. Xue, G. Yao, S. Zheng, A facile synthesis of g-C_3N_4/TiO_2 hybrid photocatalysts by sol-gel method and its enhanced photodegradation towards methylene blue under visible light, Adv. Powder. Technol. 27 (2016) 330–337.
[28] X. Zhong, M. Jin, H. Dong, L. Liu, L. Wang, H. Yu, S. Leng, G. Zhuang, X. Li, J.G. Wang, TiO_2 nanobelts with a uniform coating of g-C_3N_4 as a highly effective heterostructure for enhanced photocatalytic activities, J. Solid. State. Chem. 220 (2014) 54–59.
[29] J. Wang, J. Huang, H. Xie, A. Qu, Synthesis of g-C_3N_4/TiO_2 with enhanced photocatalytic activity for H_2 evolution by a simple method, Int. J. Hydrogen. Energy 39 (2014) 6354–6363.
[30] X. Chen, J. Wei, R. Hou, Y. Liang, Z. Xie, Y. Zhu, X. Zhang, H. Wang, Growth of g-C_3N_4 on mesoporous TiO_2 spheres with high photocatalytic activity under visible light irradiation, Appl. Catal. B 188 (2016) 342–350.
[31] J. Su, L. Zhu, P. Geng, G. Chen, Self-assembly graphitic carbon nitride quantum dots anchored on TiO_2 nanotube arrays: An efficient heterojunction for pollutants degradation under solar light, J. Hazard. Mater. 316 (2016) 159–168.
[32] B. Jurgens, E. Irran, J. Senker, P. Kroll, H. Muller, W. Schnick, Melem (2,5,8-triamino-tri-s-triazine), an important intermediate during condensation of melamine rings to graphitic carbon nitride: Synthesis, structure determination by X-ray powder diffractometry, solid-state NMR, and theoretical studies, J. Am. Chem. Soc. 125 (2003) 10288–10300.
[33] B.V. Lotsch, W. Schnick, New light on an old story: formation of melam during thermal condensation of melamine, Chemistry 13 (2007) 4956–4968.
[34] J. Yan, H. Wu, H. Chen, Y. Zhang, F. Zhang, S.F. Liu, Fabrication of TiO_2/C_3N_4 heterostructure for enhanced photocatalytic Z-scheme overall water splitting, Appl. Catal. B 191 (2016) 130–137.
[35] K. Kondo, N. Murakami, C. Ye, T. Tsubota, T. Ohno, Development of highly efficient sulfur-doped TiO_2 photocatalysts hybridized with graphitic carbon nitride, Appl. Catal. B 142 (2013) 362–367.
[36] J. Ran, G. Gao, F.T. Li, T.Y. Ma, A. Du, S.Z. Qiao, Ti_3C_2 MXene co-catalyst on metal sulfide photo-absorbers for enhanced visible-light photocatalytic hydrogen production, Nat. Commun. 8 (2017) 13907.
[37] X. Fan, Z. Xing, Z. Shu, L. Zhang, L. Wang, J. Shi, Improved photocatalytic activity of g-C_3N_4 derived from cyanamide-urea solution, RSC Adv. 5 (2015) 8323–8328.
[38] H. Zhu, D. Chen, D. Yue, Z. Wang, H. Ding, In-situ synthesis of g-C_3N_4-P25 TiO_2 composite with enhanced visible light photoactivity, J. Nanopart. Res. 16 (2014).
[39] K. Dai, L. Lu, C. Liang, Q. Liu, G. Zhu, Heterojunction of facet coupled g-C_3N_4/surface-fluorinated TiO_2 nanosheets for organic pollutants degradation under visible LED light irradiation, Appl. Catal. B 156 (2014) 331–340.
[40] W.K. Jo, T.S. Natarajan, Influence of TiO_2 morphology on the photocatalytic efficiency of direct Z-scheme g-C_3N_4/TiO_2 photocatalysts for isoniazid degradation, Chem. Eng. J. 281 (2015) 549–565.
[41] Z. Wei, F. Liang, Y. Liu, W. Luo, J. Wang, W. Yao, Y. Zhu, Photoelectrocatalytic degradation of phenol-containing wastewater by TiO_2/g-C_3N_4 hybrid heterostructure thin film, Appl. Catal. B 201 (2017) 600–606.
[42] X. Song, Y. Hu, M. Zheng, C. Wei, Solvent-free in situ synthesis of g-C_3N_4/{001}TiO_2 composite with enhanced UV- and visible-light photocatalytic activity for NO oxidation, Appl. Catal. B 182 (2016) 587–597.
[43] K. Sridharan, E. Jang, T.J. Park, Novel visible light active graphitic C_3N_4-TiO_2 composite photocatalyst: synergistic synthesis, growth and photocatalytic treatment of hazardous pollutants, Appl. Catal. B 142 (2013) 718–728.
[44] S. Zhou, Y. Liu, J. Li, Y. Wang, G. Jiang, Z. Zhao, D. Wang, A. Duan, J. Liu, Y. Wei, Facile in situ synthesis of graphitic carbon nitride (g-C_3N_4)-N-TiO_2 heterojunction as an efficient photocatalyst for the selective photoreduction of CO_2 to CO, Appl. Catal. B 158 (2014) 20–29.
[45] J. Ma, X. Tan, T. Yu, X. Li, Fabrication of g-C_3N_4/TiO_2 hierarchical spheres with reactive {001} TiO_2 crystal facets and its visible-light photocatalytic activity, Int. J. Hydrogen. Energy 41 (2016) 3877–3887.
[46] R. Hao, G. Wang, H. Tang, L. Sun, C. Xu, D. Han, Template-free preparation of macro/mesoporous g-C_3N_4/TiO_2 heterojunction photocatalysts with enhanced visible light photocatalytic activity, Appl. Catal. B 187 (2016) 47–58.
[47] B. Sun, N. Lu, Y. Su, H. Yu, X. Meng, Z. Gao, Decoration of TiO_2 nanotube arrays by graphitic-C_3N_4 quantum dots with improved photoelectrocatalytic performance, Appl. Surf. Sci. 394 (2017) 479–487.
[48] W. Chen, T.Y. Liu, T. Huang, X.H. Liu, G.R. Duan, X.J. Yang, S.M. Chen, A novel yet simple strategy to fabricate visible light responsive C, N-TiO_2/g-C_3N_4 heterostructures with significantly enhanced photocatalytic hydrogen generation, RSC Adv. 5 (2015) 101214–101220.
[49] J. Ma, C. Wang, H. He, Enhanced photocatalytic oxidation of NO over g-C_3N_4-TiO_2 under UV and visible light, Appl. Catal. B 184 (2016) 28–34.
[50] G. Dai, T. Wang, S. Liu, Y. Liang, W. Xu, Self-generated macrochannel-structure TiO_2/g-C_3N_4 with high photocatalytic activity, Aust. J. Chem. 69 (2016) 478–484.
[51] Y. Zang, L. Li, Y. Xu, Y. Zuo, G. Li, Hybridization of brookite TiO_2 with g-C_3N_4: a visible-light-driven photocatalyst for As^{3+} oxidation, MO degradation and water splitting for hydrogen evolution, J. Mater. Chem. A 2 (2014) 15774–15780.